

*Approved
10/10/96
B*

**MICROSTIMULATORS AND MICROTRANSDUCERS
FOR FUNCTIONAL NEUROMUSCULAR STIMULATION**

Contract #N01-NS-5-2325
Quarterly Progress Report #7
Period: September 10, 1996 - December 9, 1996

ALFRED E. MANN FOUNDATION FOR SCIENTIFIC RESEARCH
12744 San Fernando Road, Sylmar, CA 91342
Joseph H. Schulman, Ph.D., Principal Investigator
John Gord, David Payne, Abe Smith, Cecilia Tanacs

BIO-MEDICAL ENGINEERING UNIT, QUEEN'S UNIVERSITY
Kingston, ON K7L 3N6 CANADA
Frances J.R. Richmond, Ph.D., Principal Investigator
Gerald Loeb, Kevin Hood, Ray Peck, Anne Dupont, Tiina Liinamaa

PRITZKER INSTITUTE OF MEDICAL ENGINEERING, ILLINOIS INSTITUTE OF
TECHNOLOGY
Philip R. Troyk, Ph.D., Principal Investigator

Abstract

We are developing a new class of implantable electronic devices for a wide range of neural prosthetic applications. Each implant consists of a microminiature capsule that can be injected into any desired location through a 12 gauge hypodermic needle.

Multiple implants receive power and digitally-encoded command signals from an RF field established by a single external coil. The first type of implant is a single-channel microstimulator equipped with capacitor-electrodes that store charge electrolytically and release it upon command as current-regulated stimulation pulses. We are also working on implants equipped with bidirectional telemetry that can be used to record sensory feedback or motor command signals and transmit them to the external control system.

In the past quarter, we successfully completed preclinical regulatory testing of the implant materials and submitted a journal article describing long-term active testing of our previous generation of microstimulators in cats. We are still refining the hermetic sealing and testing procedures for the current generation microstimulator, which has required additional fixturing and process control to improve reliability and yields and to reduce operator skill in preparation for conventional manufacturing. A successful series of hermetically sealed units was made just prior to the mailing of this report. A new method for humidity sensing is described. The new integrated circuits for an improved microstimulator with higher compliance voltage and a transceiver test chip for back telemetry were released to the foundry. We hope the new designs will fix a newly discovered latch-up problem discovered in the old IC chip. Various improvements have

been made to the RF coil-driver circuits and to the test accessories for the bedside controller.

Implantable Devices

Seals

The conversion of the original microtorch sealing process to a set of more reproducible laser sealing processes has continued to be more demanding than originally anticipated. The lesson learned is that it takes a great deal of carefully designed fixturing and process control automation to replace the eye-hand coordination of a skilled technologist. Nevertheless, this step is necessary in order to reliably and repeatedly make hermetic seals.

One major advance was the successful construction and installation of a computerized sequencer for laser power and beam steering, which permits easy modification, storage and recall of various weld schedules for the CO₂ infrared laser. The computer interface was built at Queen's University and the DOS software was written at the Mann Foundation. We have also added a set of floating spacers that keep the glass beads positioned in the middle of the welding zone while the assembly is being rotated to produce even heating during welding. This was particularly problematic with

the current beads, which actually consist of two concentric beads to reach the required wall thickness; a new batch of glass is on order from Kimbel to produce single beads but this will not be available until spring.

YAG laser-welds for metal-to-metal joints have been tested qualitatively as noted below; a Chatillon quantitative pull-tester is on order. These parts are now being produced in-house at Advanced Bionics Corp. using their computerized YAG laser.

The following is a list of all weld processes, their requirements and current status (numbers in parentheses are keyed to the accompanying assembly flow chart):

Ta - Pt-Ir washer (1)

This is an electromechanical connection from the stem of the Ta electrode to a contact surface that bears against the PCB in the implant. A multistation fixture has been successfully built and used to produce this weld reliably. We have recently received slightly smaller o.d. washers which will solve an occasional problem that occurred in subsequent steps when the glass capillary touched the side of the washer while forming the capsule, resulting in a mechanically weak point.

Ta - Glass bead (2)

This is a hermetic feedthrough. The computer-controlled CO2 laser schedule.

reliably produces low-stress seals between the glass bead and Ta electrode stem. We have gone back to positioning the bead between the Ta slug and Pt-Ir washer so that it is not touching either surface because this avoids a poorly controlled variable that appeared to affect stress in the seals. We are still hand-polishing the Ta stem wires, which is effective in preventing low rate leaks through longitudinal scratches in the Ta wire stock, but is tedious and often bends the stem, compromising subsequent alignment in the laser chucks. Our efforts to obtain Ta slugs sintered onto smooth Ta wire stock have been stymied for the past quarter because a product liability lawyer at the wire supplier noted that the requested wire contained a tiny amount of silicon as a crystal grain dopant to improve its anodization properties. This lawyer decided that silicon sounded too much like silicone for them to want to supply the wire for medical use. A supplier of appropriately surfaced silicon-free Ta wire has now been located. When the sintered slugs are obtained (probably early February), we will need to repeat the electrical leakage tests after anodization, but we believe that they are unlikely to be affected significantly by the tiny surface of wire actually exposed.

Glass-glass capsule subassembly (3)

This is an open-ended capsule with Ta-electrode feedthrough at one end. The laser welder is used to melt the end of a precut length of glass capillary to the glass bead melted onto the Ta stem in the previous step. Improved collets and computer control of the laser now reliably produce a low-stress and hermetic capsule subassembly at the

limits of testing in our helium leak apparatus (now down to 2×10^{-11} with various repairs, calibrations, new o-ring fixturing, liquid nitrogen trap and reduced helium background).

Pt-Ir Tube - Ir electrode (4)

This is the first step in building the feedthrough that closes the capsule and connects the electronics to the Ir electrode. The YAG-laser weld involves an oblique melt of the Ir washer to the side of the tube without puncturing the tube. We have now obtained washers that fit snugly enough to permit this weld to be produced reliably in a multistation fixture. Previously, we have made this weld from the side of the washer that faced the glass bead that is melted onto the tube in the next process. However, we noted that the laser melt produced an irregular surface on the Pt-Ir tube that sometimes extended under the glass bead and appeared to be responsible for a stress-riser that could result in stress fractures of the bead during later processing. We have now turned the weld around so that the scarred portion of the tube is the external portion that is eventually cut off after being used as a handle for fixturing and leak-testing.

PtIr Tube - Pt-Ir washer (5)

This is the electromechanical counterpart to the Ta-PtIr washer in the capsule subassembly, making contact to the PCB via a compression spring. The Pt-Ir washer is YAG laser-welded to the open end of the Pt-Ir tube, maintaining patency of the tube so that it can be used for vacuum bake-out and backfilling with inert gas during the final

sealing process. The i.d. of the washer is critical for a close fit and the o.d. has been reduced to avoid the same problem with glass touching the washer as was noted at the Ta end. These welds are now being produced reliably in a multistation fixture.

Pt-Ir Tube - Glass bead (6)

This is a hermetic feedthrough. The glass bead is now being melted onto the middle of the Pt-Ir tube, with care taken to avoid touching either the Pt-Ir or Ir washers for the same reason noted above for the Ta end. This seal is probably the most critical in terms of obtaining sufficient compression stress to assure hermeticity but not so much as to produce stress fractures. Computer control of the laser has been essential for producing reproducible results as measured by photoelastic stress, but larger numbers of test parts will be needed to optimize weld schedules. In general, higher heat during the sealing process results in higher compression stress, which is paradoxical given the fact that the thermal coefficient of Pt-10Ir ($8.7 \times 10^{-6}/^{\circ}\text{C}$) is substantially higher than the N51A borosilicate glass (5.5) and the tube is hollow and compressible. This is in agreement, however, with the fact that the nominally more compatible R6 soda lime glass (9.3) produced very high compression stress and rapid stress fracturing of those beads when tested previously. The likely explanation is in the nonlinearities of the glass thermal coefficients for different ranges of softening and annealing temperatures.

Glass-glass capsule closure (7)

The electronic subassembly is sealed into the capsule by melting the end of the glass capillary of the capsule subassembly onto the glass bead on the Pt-Ir tube, in a weld that is similar to the Ta capsule subassembly. This weld is relatively easy to make, but there are a number of complex interactions with the condition of the glass bead left in the previous step and the outside profile of the glass capillary, which needs to avoid protrusions in order to slip through the 12 gauge implantation tool. It is desirable to minimize heating of the glass bead, both to prevent stress build-up on the Pt-Ir tube and to minimize heat conducted to the internal spring that abuts the Pt-Ir washer. One problem that was noted recently is a lensing effect, whereby poorly focussed infrared light passing through the glass bead may be concentrated near the surface of the Pt-Ir tube at the center of the bead. Improved focussing of the laser beam and steering and computer control of power have now provided reproducible results, but we have not completed a sufficient number of parts to optimize the weld schedule plus other variables such as amount of overlap between the glass capillary and bead (which can be adjusted by a horizontal stepping motor on one chuck that produces more or less compression of the spring).

Pt-Ir Tube final seal (8)

This is the final hermetic seal after vacuum bake-out and backfilling with inert

gas. A number of completed capsules that tested hermetic at the end of the glass sealing steps developed gross leaks and/or electrical shorts after this final, supposedly innocuous step. A soft Pt wire is inserted into the open outside end of the Pt-Ir tube, the tube is cut off flush with the Ir electrode, and the end is YAG laser-sealed shut in a mixture of helium and argon after vacuum bake-out. The electrical shorts were traced to inserting the wire too deeply into the tubing, permitting it to touch the end of the PCB inside the capsule. The loss of hermeticity appears to be related to mechanical shock of the interface between the glass bead and Pt-Ir tubing produced when using mechanical cutters on the tubing only 0.5 mm away from this compression seal. In preliminary tests, we found it easy to use the YAG laser to cut off the tube and weld it shut in one operation. A multistation fixture is now under construction. A similar approach will probably be used to trim the Ta stem and weld it to the Pt-Ir washer (weld 1 on figure) in one operation.

Hermeticity testing

The Alcatel helium leak tester in use has been refurbished and refitted with custom-designed o-ring ports that provide reasonably rapid and safe testing of the seals at those stages of the assembly process that permit fixturing onto the glass capillary tubing or the Pt-Ir tubing. Nevertheless, this is a tedious procedure that risks contaminating and even damaging completed devices and it has limitations as a final test after the capsule is sealed. We are back-filling the glass capsule with a helium-argon mixture that permits testing for low helium leak rates by fixturing alternately on each end of the glass capsule,

but this doesn't work for gross leaks that result from cracked glass because the helium leaks away before it can be measured. Gross leaks are typically detected in hot Freon bubble testers, but our commercial equipment is geared for small numbers of large parts rather than large numbers of small parts like the microstimulators. For these reasons, we are adapting a new design developed by Chuck Byers at the Mann Foundation, in which a large number of individual hermetic devices can be bomb-tested simultaneously in a fixture that provides an excellent microscopic view of each seal. It is hoped that this type of batch testing will eventually replace all individual seal testing during production, but the sensitivity of this test is unlikely to be as high as conventional helium mass-spectrometer testing, particularly at the tantalum end where the sintered material tends to trap helium. The design and validation of the new leak tester will be presented in the next QPR. In preparation for that development, we have reviewed the leak-testing requirement in light of the performance of the getter material described in our previous QPRs:

The internal volume of the microstimulator capsule is estimated at 0.01 cc (1.6 mm i.d. x 10 mm long, 50% filled). If there is no initially present water or water gettering, failure is anticipated when sufficient water vapor leaks in to reach saturation at 37°C (6% relative humidity). This can be converted into an equivalent helium leak volume by multiplying by the square root of the ratio of molecular weights of water vs. helium (2.12), resulting in 1.3×10^{-3} cc He. For a 10 year functional life (3×10^8 s), the leak rate must be below 4×10^{-12} cc atm/s

He, which is lower than is practical to measure except with specially designed moisture sensor chips (which we are developing in order to test the limits of capsule hermeticity but which are not suitable for production testing).

The getter that we have chosen is anhydrous magnesium sulfate (120 g/mole), which is fully hydrated at 8 moles water per mole of salt. The getter produced in our previous feasibility study, which will fit in with our current electronic subassembly, has a volume of 0.56 mm^3 with an anhydrous salt concentration of $1.7 \mu\text{g}/\text{mm}^3$. With a proposed new electronic subassembly, we expect to use a cylindrical getter that is 1 mm long x 1.4 mm o.d. x 0.5 mm i.d., resulting in a volume of $1.34 \text{ mm}^3 = 2.3 \mu\text{g salt} = 2 \times 10^{-5}$ moles. When fully hydrated, this salt would absorb 16×10^{-5} moles water or 3.6 cc water vapor at standard temperature and pressure. This translates to 7.63 cc helium, permitting a leak rate of 2.5×10^{-8} cc atm/s He (for 10 year survival), which is readily measurable in helium leak testers and at the edge for conventional bubble testers. A more conservative position would probably down-rate the permissible leak by a factor of 2 (to avoid full saturation of the getter) and by a further factor of 2.5 until we can use the larger getter, resulting in 5×10^{-9} cc atm/s He. The improved bubble tester is expected to be practical for leak rates below 1×10^{-9} , with no upper limit, so it should be a suitable production replacement for the various individual tests now being used during development of the manufacturing processes.

Moisture sensing

As part of our plan to detect residual moisture and slow leaks in sealed glass capsules, we intended to fabricate an aluminum-on-quartz comb pattern, identical in size to the microstimulator chip, and use the pattern as a moisture detector. Each side of the comb would be connected to an existing microstimulator electrode and we intended to use Impedance Spectroscopy to sense the condensation of water on the pattern.

Upon examination of the micro-printed-wiring board (uPWB) normally used within the microstimulator, it was noticed that the traces of that board might be suitable for use as a moisture sensor. We have measured the impedance of the uPWB under 28% and 88% RH conditions and we find that there is a measurable impedance value which changes with variations in RH. Based upon this early, but promising testing, we are fabricating a test fixture to hold the sealed glass capsules which will permit the Impedance Spectroscopy measurement. The glass capsule will be sealed with only the uPWB and the interconnection spring between the two electrodes. By connecting the Impedance Spectroscopy testing system between the two microstimulator electrodes it should be possible to observe any increase in residual moisture within the glass capsule.

ASIC

Integrated circuit latchup

At IIT, during the design and testing process for extracorporeal transmitters, it was noticed that some microstimulators displayed intermittent and variable operation. A microstimulator which would work at one setting of transmitter current and modulation would subsequently cease operation while being excited under identical conditions. Microstimulators and transmitters which were shipped to Queen's would often fail to operate upon arrival, despite thorough check-out at IIT. Initially it was thought that this behavior was caused by the use of triangular, variable-baseline, modulation in the Class-E transmitters. Therefore, we revised the transmitter circuits to produce square-wave modulation. The circuitry necessary to produce the square-wave modulation had been previously designed and was included in the printed-wiring-board layout. We had omitted the components from the transmitters which we had recently built because earlier testing with the 9cm-diameter helical coil had showed that the triangular modulation was able to reliably control the prototype microstimulator devices. Further testing with more microstimulators and different transmitter coil configurations exposed the intermittent microstimulator behavior.

After extensive bench testing, it was discovered that using square-modulation did not eliminate the problem. In the recent group of microstimulator electronic submodules,

sent to IIT for test, 10 out of 15 devices exhibited the intermittent behavior. Upon close examination, it was observed that the integrated circuit could switch to a “latched” mode of operation. In this latched mode, it would not respond to any command sequences, and would not produce sufficient compliance voltage for proper chip operation. Furthermore, the onset of the latched behavior was influenced by the rate at which the magnitude of the exciting field was increased. While holding the electronic module in one’s hand, and slowly moving towards the transmitter coil, (with the module in a test fixture) the latched behavior could be observed on an oscilloscope.

At this point we are awaiting the results of duplicate testing at the Mann Foundation. While the precise cause of the latch behavior is unknown, we expect that it is peculiar to this chip design. Probing of the chip to determine the exact cause is a time-consuming task. The recently designed microstimulator integrated circuit, which has been submitted to AMI, will in all probability not duplicate this problem due to the radical differences in the circuit designs. Therefore we intend to wait for the new AMI chips to be delivered, or wait for further test data from the Mann Foundation before considering this problem or new transmitter designs further.

The new microstimulator chip and the transceiver test chip were released to the foundry at the end of this quarter after one final delay for relayout. The original specification for the chips was a width of 43 mils, but this crept up to 47 mils after process-dependent guard bands were added in final layout. It was decided that this width

would result in stack-up tolerances that would seriously constrain work in progress to automate the manufacture of the electronic subassemblies, so another set of layouts was done with 38 mil widths. This, however, resulted in loss of some of the conservative barrier regions between high-voltage gates in the transceiver test circuits. In the event, we designed a mixed reticle with 17 versions of the 38 mil wide microstimulator (16 preset addresses plus one laser-programmable address), a 38 mil wide transceiver design, and a 47 mil version of the transceiver. The reticles were spaced so that a constant step in the dicing process would recover all of the microstimulator chips, sacrificing the wider transceiver chip. The relatively small numbers of transceiver chips actually needed will be obtained by manually dicing the desired rows of the wafer.

Some of the spice simulation parameters that were needed to understand the circuit thoroughly were in doubt after conversations with foundry engineers. As insurance against a possible requirement for another iteration, a set of sample components and circuit elements were also included on this foundry run to eliminate any modeling doubts on future runs.

Testwell Accessories

The drywell test station is an accessory to the bedside controller that allows the clinician to find the address and verify that the microstimulator is functional while it is

still in its sterile container. It consists of a pair of capacitive pick-up electrodes that surround the cylindrical container containing the implant, plus amplification and detection circuitry to respond to the voltage swing produced at the output electrodes in response to a valid command signal from a nearby RF transmission coil. The first design used differential amplification and careful positioning of the pickup electrodes and transmission coil so that the RF field produced by the carrier was small compared to the output pulse of the implant. This placed an undue burden on the mechanical design of the accessory and RF coils. In the new circuit, a 2 Mhz LC notch filter is used in front of a single-ended instrumentation amplifier. This amplifier module is now built into the connector that plugs into the bedside controller, moving it away from the magnetic fields near the drywell itself. The gain of the preamplifier boosts the signal to the same range as produced by a microstimulator in a wetwell test accessory, which measures output current of an individual implant quantitatively by recording the voltage drop in a narrow, saline-filled well equipped with two recording electrodes. Thus, the same pulse detection and digitization circuitry in the bedside controller (and, in fact, the same input jack) can be used for either test function. Work is underway to unify our present Windows software and microprocessor firmware so that both benchtop calibration tests and clinical address tests can be conducted from the same platform.

Preclinical Regulatory Testing

All passive materials compatibility testing is now complete and all tests were passed, including cytotoxicity, systemic toxicity, sensitization, intracutaneous toxicity, and mutagenicity (Ames test, sister chromatid exchange test and chromosomal aberration test). Fabrication of dummy and active implants for chronic in vivo testing has been delayed until all sealing processes have been stabilized.

The results of long-term active in vivo testing of our first generation microstimulators are detailed in the appended journal article by Cameron, Liinamaa, Loeb and Richmond, entitled “Long-term biocompatibility of a miniature stimulator implanted in feline hind limb muscles.” It includes quantitative histological analysis demonstrating that both active and passive microstimulators produce foreign body reactions that are remarkably similar to conventional biocompatible materials such as nonadsorbable sutures. This article and the companion appended to our previous QPR by Cameron, Richmond and Loeb on “Effects of regional stimulation using a miniature stimulator implanted in feline posterior biceps femoris” have been submitted to IEEE Trans. Biomedical Engineering.

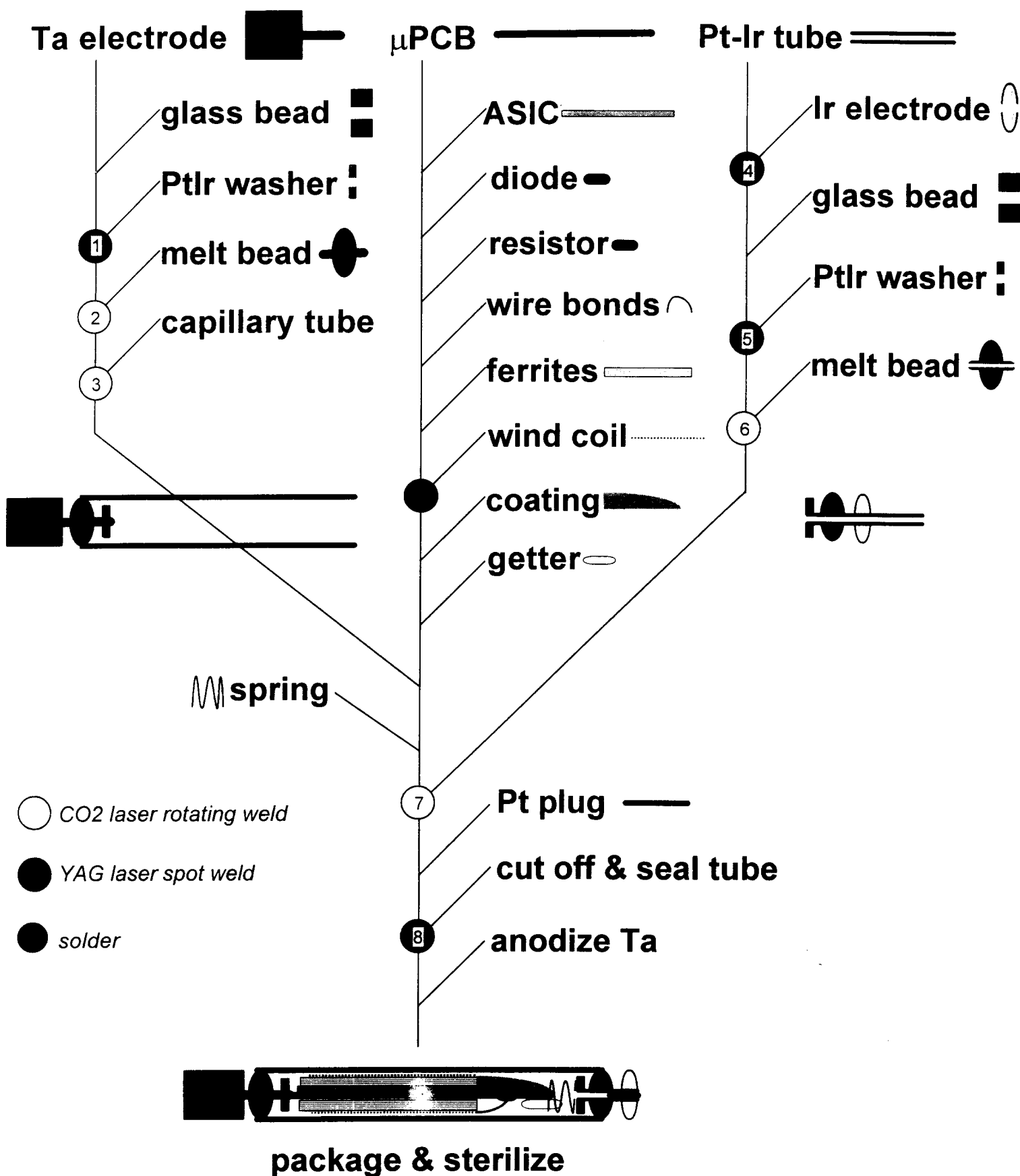
During November-December, Francesco Palazzo, a visiting graduate student from Milan Polytechnic University, worked on the design of insertion strategies and transmitting antennas for clinical use of microstimulators to aid in post-operative

rehabilitation of patients undergoing hip replacement. Cadaver dissections and models of the implant site were used to identify target neuromuscular compartments and landmarks for percutaneous insertion of microstimulators. A model of the microstimulator equipped with percutaneous wire leads was build for acute intraoperative testing of these approaches by Dr. Carlo Romano, the orthopedic surgeon who is developing this clinical application. Mr. Palazzo also demonstrated that the presence of various metallic hip implants did not adversely affect the ability to provide RF power and control for adjacent microstimulators.

Plans for Next Quarter

In the next quarter, we intend to finalize and validate the sealing process and provide the necessary dummy and active implants to support preclinical chronic animal tests that are funded under other auspices and the long-term in vitro tests that are part of this contract. We expect to receive and test the new ASICs from the foundry, which should provide sufficient information to proceed with definitive design of the bidirectional telemetry scheme required for the microtelemetry implants.

BION™ Implant Assembly Sequence



**LONG-TERM BIOCOMPATIBILITY OF A MINIATURE STIMULATOR
IMPLANTED IN FELINE HIND LIMB MUSCLES**

T.Cameron, T.L. Liinamaa, G.E.Loeb, and F.J.R.Richmond

Queen's University, Kingston, Ontario, K7L 2N6

Tracy Cameron at University of Alberta, 513 Heritage Medical Research Centre, Edmonton,
AB, T6G 2S2; phone (403)492-1616; FAX (403)492-1617; e-mail tracy@biomed.queensu.ca

Submitted

ABSTRACT

Chronic foreign-body responses and muscular changes were examined following the implantation of active miniature stimulators into the hind limb muscles of cats for periods of up to 3 months. The RF-powered stimulators were injected into muscles through a 12-gauge hypodermic needle. The tissue responses around the active stimulators were compared histologically to those provoked by passive devices, broken glass, silicone tubing, polyester suture material coated with polybutylate, and two of the internal components of the stimulator (ferrite, integrated circuit chip). Active and passive stimulators produced similar, benign foreign-body reactions that resulted in an essentially identical fibrous capsule over time. The responses were similar to those produced by the internal components and the suture material, and were more modest than those produced by the broken glass. The capsule did not appear to interfere with the functionality of active devices because thresholds measured during the post-implantation survival period did not change significantly over time. Unexpectedly, the severity of the reaction differed significantly amongst the various target muscles. Medial gastrocnemius exhibited the most severe response whereas tibialis anterior had the least reaction.

INTRODUCTION

In clinical practice, devices that apply electrical stimulation to muscles most commonly use electrodes placed on the skin to deliver the stimulus pulses. However, advances in microtechnology now make it possible to construct implantable stimulators that can be inserted directly into muscles or next to nerves. One such miniature device consists of a cylindrical glass package with an electrode sealed hermetically into each end [1], [2]. It receives power and data from a single amplitude-modulated radio-frequency (RF) field via inductive coupling. This new technology eliminates many of the problems encountered with surface stimulation. However, all implanted medical devices are foreign bodies that trigger tissue changes whose effect on device performance and the health of the recipient must be understood before they can be used clinically.

One method used to assess the biocompatibility of an implanted device is to evaluate the tissue response using light microscopy. Tissue implanted with a foreign body undergoes a series of inflammatory reactions that occur, in part, as a response to the surgical process itself. During the first 24 to 48 hours following implantation, tissue can show redness (due to local vascular dilation), heat (due to increased local blood flow), swelling (due to increased local vascular permeability), and pain (due to local accumulation of chemical mediators) [3]. The severity of the inflammatory response is thought to be related to the nature of the protein layer formed on the surface of the implant [4], [5]. The type of protein that most readily adsorbs onto the surface of an implant will depend on the materials composing the implant [6], [7]. For example, proteins

such as albumin do not contribute to the inflammatory response [8] whereas fibrinogen can elicit the accumulation of large numbers of phagocytic cells [9].

The acute inflammatory response usually resolves after about a week. Over subsequent months, the implant becomes encapsulated by a progressively more fibrous layer of connective tissue [3]. If the device is highly biocompatible, the capsule is generally quite thin, and the interspace between it and the device contains only a few macrophages. When devices provoke continued tissue reaction, the surrounding connective tissues are thicker, more vascularized and disorganized and they contain large numbers of necrotic cells and leukocytes. The continued presence of leukocytes indicates possible infection and/or biological degradation of the implant itself.

The surface materials of the new implantable stimulator tested in this study [1] are borosilicate glass and tantalum and iridium metal. Individually these materials have been found to be highly biocompatible [10], [11], [12], [13]. In a recent study, Fitzpatrick et al. [14] showed further that a stable, fibrous capsule formed around similarly shaped but passive glass devices and stimulators that were implanted in muscle for a period of two months.

In this study, we examined the long-term performance as well as the tissue response of active and passive miniature stimulators. First, we used histological methods to compare the tissue responses around the active stimulators to those provoked by passive devices, broken glass, silicone tubing, polyester suture material coated with polybutylate, and two of the internal components of the stimulator [ferrite, integrated circuit (IC) chip]. This was done by implanting the materials into hind limb muscles of cats for periods of up to 3 months. Second, we examined the long-term performance of the stimulator by measuring thresholds of stimulation for muscle,

weekly, over this period. Our results showed that active and passive miniature stimulators elicit similar, benign foreign body reactions, that progress to form essentially identical fibrous capsules over time. This reaction did not appear to interfere with the functionality of the device because thresholds measured during chronic implantation did not change significantly over time. We did find, however, that the severity of the reaction appeared to differ amongst the various host muscles.

MATERIALS AND METHODS

Surgical preparation

Experiments were carried out on nine cats (2.8-4.2 kg; either sex) anesthetized with sodium pentobarbital (initial dose, 35 mg / kg ip; supplemental doses, 5 mg / kg iv). Cats were placed in one of two groups to test the biocompatibility of devices (n=4) or components (n=5). In each cat of series A, four active devices were implanted using aseptic techniques in right hindlimb muscles and four passive devices were placed in the comparable left hindlimb muscles (Table 1A). In each cat of series B, muscles in each hindlimb were implanted with passive devices, silicone tubing (Silastic, Dow Corning, Midland, MI), broken glass tubing of the kind used in the external capsule (Kimbel borosilicate glass type N51A; Friedrich & Dimmock), or one of two internal components (integrated circuit chips or ferrite pieces)(Table 1B). To insert the tested devices or components two skin incisions were made in each limb. One incision extended along the anterior surface of the shank, and the other along the posterior surface from the popliteal fossa to the calcaneum. In all but one animal in series A, devices or components were inserted parallel to the muscle fibers in each of the following muscles: tibialis anterior (TA), extensor digitorum longus (EDL), medial gastrocnemius (MG), and either soleus or lateral gastrocnemius (LG). In one cat of series A, active and passive devices were implanted into the semitendinosus, biceps femoris, and anterior and medial sartorius muscles of a single cat. This latter procedure was performed to assess any differences in tissue reactions between muscles with in-series versus pinnate fiber architectures. In all cases intact devices were injected using a 12 gauge angiocath insertion tool (Becton Dickinson Vascular Access; Sandy, Utah). Components were introduced

by making a small channel in the muscle tissue by blunt dissection with fine scissors and inserting the device with fine forceps. A single suture (6-0 Ethibond, Ethicon) was tied at the muscle-entry site to prevent the device from migrating out of the muscle, and to aid in locating the device at the time of removal.

Stimulation

Animals were trained to recline in a tube (8 inches diameter x 18 inches long) for two hours a day by using palatable food as an incentive. The transmitting coil that sent data and power to the implant was wrapped around the outside of the tube. After surgery the animals recovered for three to five days. Stimulation settings (pulse width and current amplitudes) required to produce threshold twitches of the muscle were determined for each active device. Current twice or four times threshold was used during daily stimulation, applied while alert animals fed or rested in the tube (Table 1). Each device was activated at 4 sec intervals using trains of stimuli at 20 Hz for 1 sec. Stimulators were activated in pairs (one flexor and one extensor) producing co-contractions, thus reducing the movement of the limb. Stimulus trains were applied for two hours a day, five days a week, for a period of up to three months.

Weekly measurements

Once a week, threshold measurements were made for all implanted active devices. Animals were anaesthetized using intramuscular injection of ketamine hydrochloride (Rogarsetic, Rogar/STB Inc.; 9 mg / kg) and xylazine (Rompun, Haver; 0.5 mg / kg) to eliminate voluntary muscle contractions. Thresholds were obtained by setting the current amplitude to the lowest

setting still able to produce a palpable muscle twitch using the maximal pulse width of 258 μsec .

The pulse width was decreased in one μsec steps, until the twitch was no longer detected.

Terminal measurements

For the terminal procedure, two cats were anaesthetized by intravenous injection of sodium pentobarbital (as above). TA and EDL muscles were removed from the distal insertion and attached to a strain gauge (Figure 1). Isometric twitch and train forces were measured using a force transducer (measured linear up to 35 N; compliance 8.9 $\mu\text{m/N}$) attached to the tendon of insertion. The force transducer was attached to a motor-driven puller that was used to adjust whole-muscle length. A bone screw was fastened to the tibia and fibula and secured to the frame of the puller to fix the origins of the muscles. Contractions were elicited by stimulating muscle nerves either with the implanted stimulator or from the sciatic nerve using a nerve cuff. This allowed comparison of the maximal force output of each muscle produced by an active device with that produced using a nerve cuff.

All implants were removed from the animals and examined under a dissecting microscope and environmental scanning electron microscope (ESEM; model E-3, Electroscan) for any visible damage or changes in surface characteristics. These results are discussed in a previous report [2].

Tissue processing

Each muscle was weighed and cut into small transverse blocks (2 cm x 2 cm x 2 cm). The blocks were mounted on aluminum disks using embedding medium (OCT compound, Ames) and

the orientation of each block was recorded. Muscle blocks were coated with talcum powder and immersed into liquid nitrogen (-196°C) for storage. The blocks were warmed to -20°C and cut into 15-18 μm transverse sections. Two or more adjacent cryostat sections were retained at 2 mm intervals. Sections were placed on gelatin coated slides and dried in a 60°C oven for 30 minutes. The tissue was stained with either haematoxylin and eosin (H&E) or picrosirius red [15]. At least one additional section was taken from each block and stained for adenosine triphosphatase (ATPase) activity after formalin fixation and alkaline (pH 10.4) preincubation [16]. Stained muscle sections were examined under a light microscope.

Data analysis

The cellular reaction and the overall tissue response to the implants and the coated suture material (6-0 Ethibond, Ethicon) marking the site of muscle entry were examined using a light microscope. Within the reactive zone counts were made of polymorphonuclear leukocytes (PMNs), lymphocytes and plasma cells, macrophages, fibroblasts, and giant cells. Cells were counted in five randomly selected 0.01 mm^2 regions within the capsule on each slide under 1000 X magnification by two investigators, one of whom was double-blinded. Results of the observations were reviewed with a neuropathologist (J. Rossiter, Queen's University). The cell counts were given a score ranging from zero to four [adapted from American Society for Testing and Materials (ASTM) standards, Vol 13.01; see Table 2], recorded on a score sheet, and the scores from the five sites were averaged. An overall cell score was calculated by multiplying each individual cell score by a weight factor. Weight factors were assigned in a manner that

reflected the significance of a particular cell type in the inflammatory response, and adapted from the ASTM standards (Vol 13.01).

The implant site was further evaluated for fibrosis and abnormal muscle fiber characteristics (Figure 2). A quantitative score from zero to four was assigned, with zero being not present and four being a severe reaction. The fibrosis score was determined by examining the thickness of the endomysium and perimysium in the tissue surrounding the implant. A score of 1 (minimum) was assigned when less than 50 cells in the perimeter of the capsule were surrounded by thickened connective tissue (greater than $10\text{ }\mu\text{m}$ thick). A score of 2 (mild) was assigned when 50 to 100 cells were surrounded by thickened connective tissue. A score of 3 (moderate) was assigned when greater than 100 cells were surrounded by thickened connective tissue. Finally, a score of 4 (severe) was assigned when most of the cells around the perimeter of the implant ($>75\%$) were surrounded by thickened connective tissue. Muscle fiber characteristics, such as size, ATPase staining, and location of myonuclei, were examined in two sites, one less than $100\text{ }\mu\text{m}$ and the other greater than $100\text{ }\mu\text{m}$ from the implant. Abnormal muscle fibers were identified by their rounded shape, small ($< 50\text{ }\mu\text{m}$) size, and/or centrally located nuclei. A score of 1 (minimum) was assigned when only a small localized region of abnormal fibers (< 50 cells) was observed and there still existed a distinct boundary between muscle fibers and capsule. A score of 2 (mild) was assigned when a larger number of non-localized muscle fibers (50 - 100 cells) appeared abnormal, and when some of these fibers (<20 cells) were separated from other fibers by connective tissue. A score of 3 (moderate) was assigned when more than 50% of the perimeter of the implant was surrounded by abnormal muscle fibers, many of which (< 50 cells) were surrounded by a thick ($<10\text{ }\mu\text{m}$), cellular connective tissue and inflammatory cells appeared

to invade some of the muscle fascicles. Finally, a score of 4 (severe) was assigned when greater than 75% of the perimeter was surrounded by abnormal muscle fibers, separated by large amounts of connective tissue ($> 10 \mu\text{m}$), and when muscle fibers and inflammatory cells were loosely mixed. A single score to reflect muscle-fiber characteristics was calculated by multiplying the two scores from different sites by a weight factor. A factor of 2 was used for sites less than $100 \mu\text{m}$ from the capsule, and a factor of 3 was used for sites greater than $100 \mu\text{m}$ from the capsule. A large weight was given for damage seen further away from the capsule, because changes would indicate a more severe response. Finally, a measurement was made of the capsule thickness by first drawing the implant site under 250X or 400X magnification using a camera lucida attachment on a microscope, and then digitizing the traces using the frame-grabbing software, BioScan Optima (version 2). The capsule thickness measurement included a thin fibrous layer surrounding a thicker cellular region. An average of five measurements was recorded for each section through an implant site. When the capsule was situated on the perimeter of the muscle, part of the capsule was often torn or folded blurring the extent of the capsule and prohibiting thickness measurements. These regions were not analyzed quantitatively.

We tested for any differences between the severity of the reaction, assessed by quantitative scores, and the type of implant or type of host muscle by performing two-sample t-tests, and one-way ANOVA using statistical functions in Excel. We grouped the muscles according to whether they had active or passive device implants and tested for any changes in the various scores over time by performing linear regression on data from cats euthanized at different survival times. The results were plotted using a Sigma plot graphing package.

RESULTS

Observations of device performance: In Situ

All devices that were activated by RF coupling caused muscle contractions that could be readily palpated through the skin. The contractions were well tolerated by the cats, who showed little interest in their moving limb and commonly slept during the stimulation session. In a single instance in which an active device was placed into the right semitendinosus, the cat began to lick a circumscribed region of skin over the posterior surface of the right hindlimb about four weeks post-implantation. The cat showed no other signs of sensitivity or gait disturbance. Nevertheless, the fact that attention was focused by the cat on this site was so unusual that the experiment was interrupted at 5 weeks to look for a source of irritation that might explain this behavior. Histological examination of the implanted muscle revealed a circumscribed but unusual pattern of damage in the right semitendinosus muscle, described below.

Of the 12 active devices that were implanted, only 1 stopped working before the end of the experiment (for summary see Table 1). This failure was due to a leak in the glass seal that allowed body fluids to enter the device and short circuit the electronics. During the course of each experiment, device functionality was assessed during the sessions at which weekly thresholds were measured for each implanted device. Figure 2 shows those measurements normalized to the values on day one for eight devices implanted into the hindlimb muscles of two cats for approximately three months. No relationship was found between the threshold measurements and the number of days that the devices were implanted, as determined by calculating the correlation coefficient for the data corresponding to each device.

Twitch forces measured during the terminal experiments for two cats implanted with active devices were calculated to be approximately 10 % of maximum. In one cat stimulated chronically at 2 x threshold, the twitch force was 13.8 % of maximum in the EDL muscle and 6.5 % in the TA muscle. In another cat, stimulated at 4 x threshold, twitch forces of 10 % were recorded in soleus, and forces of 26 % were recorded in TA.

Tissue responses:

1) Active and passive devices

All implanted devices triggered a benign inflammatory response similar to that described previously for miniature stimulators and glass capsules with similar dimensions [14]. Devices removed after 30, 56 and 100 days were surrounded by a well defined outer capsule that contained an accumulation of macrophages and leukocytes (Figure 3). Inspection of sections cut at different levels along the length of the device, from the tantalum to the iridium end, did not show any consistent differences in capsule thickness or cellular accumulations.

Analysis of foreign-body reactions focused upon two types of changes: changes that occurred in normally present tissues, including muscle fibers and connective tissues; and features of new tissues provoked by the inflammatory reaction. Examinations of muscle and connective tissues suggested that devices had modest effects that did not differ significantly for active or passive devices. ATPase staining of fibers revealed the presence of three distinct fiber types whose relative proportions were similar when fascicles abutting the fibrous capsule were compared to fascicles further from the implant site. In addition, muscle fibers immediately adjacent to the capsule surrounding a device were usually normal in size and pattern of

nucleation (Figure 3). Less than 10% of fibers abutting the fibrous capsule had cross-sectional diameters less than 50 μm or had centrally placed nuclei, as shown in Figure 3B and 3C. When atrophic fibers were seen, they were often confined to a single fascicle in which all fibers were shrunken. The enzyme profiles of these shrunken fibers were similar to those of nearby large fibers, and the fascicle displayed a similar mosaic of fiber types.

Although changes in muscle fibers were infrequent in all muscles, significant differences were found in the scores assigned to muscle-fiber characteristics when the various muscles chosen for implant were compared. Implant sites around devices from medial gastrocnemius had greater numbers of abnormal muscle fibers located throughout the perimeter of the capsule. Fibrosis close to the implant site was also a characteristic feature, that was similar in its appearance when sites around active and passive devices were compared. Fibrosis was generally observed to be less than 10 μm thick throughout the site, but the fibrosis score assigned to implant sites taken from soleus and medial gastrocnemius were found to be statistically higher than from lateral gastrocnemius and tibialis anterior. This was reflected in a more extensive distribution of perimysial thickening between muscle fiber fascicles in MG and soleus compared to TA.

The foreign-body reaction that surrounded the implanted devices had two main constituents, an outer, encapsulating layer of fibrous, cell-poor material, and an internal accumulation of loosely packed inflammatory cells. The fibrous capsules, which included both layers, did not differ significantly in thickness between muscles implanted with active or passive devices, or between different host muscles. Interestingly, the capsules were also similar in thickness to capsules around the suture material at the site of implant (Figure 4). Half of the capsules

surrounding the active and passive devices were under 0.24 mm, whereas half of those around suture material were under 0.27 mm. The fibrous layer component was found to be only 20% of the overall capsule thickness measurement. Thus, half of the fibrous capsule layers surrounding the active and passive devices were under 0.05 mm thickness.

Accumulations of inflammatory cells within the fibrous capsule were composed predominately of macrophages. Lymphocytes were present more rarely. They were found in occasional clumps at implant sites in which the overall reaction was judged to be most severe. The type of host muscle appeared to affect significantly the severity of the response as reflected in the significant differences between cell scores amongst the various host muscles. In order to eliminate this difference when comparing the responses of implanted active and passive devices, an additional analysis of active versus passive devices was confined to the 20 sampled sections from two active and two passive devices implanted in MG, the muscle demonstrating the most severe reaction. No significant differences were found between overall cell scores, fibrosis scores and muscle-fiber scores sampled from the sites around active and passive devices (Figure 5). However, a significant difference ($p < 0.05$) was found between the numbers of giant cells associated with active and passive devices (Figure 6B). These results must be interpreted with caution because the number of giant cells in each sample was very small and subject to potential sampling bias (active devices < 0.4 cells, passive devices < 0.1 cells, in a typical 0.01 mm^2 field). No significant differences were found for any other cell types. A typical inspected region contained less than 20 PMNs, 10 lymphocytes, 35 macrophages, and 10 fibroblasts. The number and type of cells did not change significantly in muscles implanted for 30 to 100 days.

Devices implanted into semitendinosus, biceps femoris, and anterior and medial sartorius of a single cat produced similar fibrous capsule formation as described above. However, upon examining the semitendinosus muscle under the patch of skin that the animal had been licking, we found an unusual region of damage that began at the level of the tantalum electrode (effective cathode) and extended into the interfascicular connective tissue toward the tendinous inscription that separates the two neuromuscular compartments of this muscle (Figure 7). The muscle fibers in this region appeared smaller in diameter than elsewhere in the muscle. The perimysium surrounding each fiber was thicker and more cellular than that surrounding fibers in undamaged regions of the same section.

2) Internal components and controls

When comparisons of capsule formation were extended to other implanted materials, the thickness of the fibrous capsule was found to vary with the type of implant (Figure 8). Components were surrounded by a thin connective tissue sheath containing a variety of inflammatory cells. The number of cells varied according to the type of implanted material. Glass shards and silicone tubing were implanted to act as positive and negative controls, respectively. Thus, the most severe reactions and the thickest capsules were found when broken glass was implanted. In some sections we observed up to 100 PMNs in a 0.01 mm^2 area near the centre of the reactive site. However, the glass shards were contained within a capsule and showed no signs of migrating out of the site of implantation. Components (ferrite pieces and IC chip) did not cause any observable differences in foreign-body response and the overall appearance of the capsules was identical to that described above for active and passive devices. The least severe reaction and thinnest fibrous capsule occurred around the soft silicone tubing.

The capsule thickness was measured to be only 0.05 mm and contained little if any cellular reaction. All capsules appeared to be stable except those produced by the glass shards, which showed a continuing presence of leukocytes and debris typical of a non-resolving inflammatory reaction.

DISCUSSION AND CONCLUSIONS

In the present study, we examined the foreign-body response to passive and active miniature stimulators and compared this response to that elicited by suture material, silicon tubing, broken glass capillary tubes, or internal components that comprise the stimulator. We found that active and passive devices elicited a similar reaction. Two lines of evidence led us to conclude that this reaction was stable over time. First, weekly threshold measurements for eliciting muscle contractions did not change significantly over time for any of the active devices. Second, histochemical assessments of host tissue revealed the presence of a stable foreign-body response similar to that produced by any non-toxic biomaterial [17]. We also found that the host muscle used for implantation appeared to affect the amount of damage caused by the implant. This observation is important for two reasons. First, it suggests that our results cannot be compared directly with studies in which implants are placed in paraspinal or gluteal muscles, often in other species. Second, it suggests that the specific reaction of a muscle to a relatively benign implant can depend as importantly on muscle-specific characteristics as device-specific characteristics.

Methodological considerations

The methodologies adopted in this study were chosen to facilitate the simultaneous study of several aspects of the muscle response. These modifications in experimental design must be kept in mind when comparing the results reported here with descriptions of histopathology reported typically in the literature. Most studies that assess biocompatibility use thin, paraffin-embedded sections [3]. However, in this study, frozen sections were used so that muscle fibers could be examined using histochemical methods to identify changes in enzyme profiles. These frozen

sections were up to three times thicker than sections cut typically from paraffin blocks.

Consequently, counts of inflammatory cells made on regions of similar size should be about 3 times higher than those anticipated by previous cell-scoring methods based on paraffin sections [3]. To compensate for the difference in section thickness, we adjusted our scoring methods for all cellular counts.

In addition, it was necessary to retrieve the devices prior to histological analysis. Retrieval was made difficult because the irregular shape of the device had encouraged connective tissues to envelop and anchor the device firmly, especially at its tantalum end. The elaboration of connective tissues at the tantalum end of the device is consistent with observations of connective-tissue ingrowth in other studies of chronically implanted, porous or roughened materials [17], [18]. The need to cut the connective tissues anchoring the device and drag the device through the encapsulating space probably caused local tissue disruption and redistribution of the cellular material within the capsule around the device. This disruption was felt to account, at least in part, for the relatively large standard deviation in some quantitative measures from different sampled sites.

One problem that was encountered during evaluation of histopathological changes was the relative generality of published criteria to score foreign-body responses. For example, it is a generally accepted practice to score fibrotic or muscular changes according to whether they are minimum, mild, moderate, and severe. These criteria assume a level of understanding of histopathology that may not exist amongst researchers who do not conduct such evaluations routinely. Further, it poses the potential for confusion when two different observers have slightly different interpretations about scoring criteria. Thus, we have attempted to specify in more detail

the scoring methods that we developed for the present study. The scores for fibrosis were found to be the most troublesome because the degree of perimysial thickening around the device was generally modest, and variations in perimysial thickness were common even in different parts of seemingly unaffected muscle far from the implanted site. Thus, scores for fibrosis should be interpreted cautiously.

Foreign body response elicited by implanted stimulators

Previous studies have suggested that the introduction of a nonabsorbable foreign body initially involves the death of cells and tissues. This reaction resolves over time as the material becomes encapsulated by a fibrous connective tissue coat. All of our tissue was examined one month or more following implantation, well after the time when we would expect to observe cell death. Thus, we were not surprised by the failure to see necrotic changes. Such necrotic changes should occur only in response to the release of local toxic substances, which are unlikely to come from the highly inert metals and glass comprising the casing of the stimulators. The cellular response that we did observe was consistent with that which occurs during the healing process. The most common cells were macrophages and lymphocytes, which have important roles in the repair process, and are commonly found at the site of an inflammatory response [19], [20]. In addition, we found the occasional giant cell. Giant cells are formed at sites of chronic inflammation from the fusion of monocytes, newly arriving from the blood, with aging macrophages [21]. They are found most commonly when implants have multiple filaments (e.g. sutures) or irregular surfaces. We had suspected that we might see more giant cells at the tantalum end of the electrode, because the tantalum electrode is rougher than other parts of the

stimulator, but this did not prove to be the case. However, any conclusions about giant-cell distribution must be guarded because tissue disruption during the removal of the stimulator may have obscured any changes in cellular accumulations at the tantalum end of the electrode.

Inflammation typically results in the accumulation of polymorphonuclear leukocytes (PMN). These cells are released at the site of inflammation and disappear four to six days after the cause for the inflammation had been removed [3]. Because very few of the sites implanted with microstimulators were found to contain PMNs, we concluded that the reactions were relatively stable. However, PMNs were present consistently in muscle implanted with broken glass pieces, suggesting a persistent rather than resolving inflammatory response. The continuing inflammation most likely was due to continued tissue damage caused by the movement of the sharp material within the muscle.

Stability of electrical thresholds

The above cellular responses suggest that a stable reaction occurred at the site of the active and passive stimulators. This conclusion was supported further by threshold measurements, which were not found to change significantly over time. In fact, many of the thresholds decreased when compared to threshold values measured on the first day after surgery. This improvement in threshold was thought to result from a reduction in swelling and inflammation and removal of any necrotic tissue produced by the initial insertion procedure.

There are two reasons why stimulus thresholds were considered to be a useful gauge of reaction stability. First, a gradual increase in threshold might have been prognostic for a progressive increase in capsule thickness, that might displace the stimulator away from excitable

elements over time. Second, a change in threshold might have suggested device migration. The relative stability in stimulus threshold that was in fact observed was consistent with the histopathology showing little change in the 300 μm separation created by the foreign-body response between the device and the adjacent excitable tissue. Nevertheless, the foreign-body response appeared to be an effective barrier to device migration, as has been identified elsewhere for devices of similar size [14]. Device migration was also presumably hampered by the extensive ingrowth of connective tissues around the tantalum electrode. Guyton and Hambrecht [18] reported previously that material accumulated in the pores of a tantalum electrode much like that used here. The ingrowth of tissue was found to increase the pore resistance of the electrode to 2-3 times that measured immediately after implantation. However, Guyton and Hambrecht [18] found no significant changes in the threshold of motor responses during a six-month period of testing. Both these and present results suggest that immobilization of the stimulator by the foreign-body reaction effectively prevents device migration, which would be detected by a change in threshold as the device moved closer or further from bundles of motor axons in the muscle (for further discussion see [14]). Whether this adhesion to the surrounding tissue is beneficial or detrimental to the evolution of the foreign-body response remains to be determined.

Changes in muscle fibers close to the encapsulation were generally modest. Rarely did a muscle fascicle contain fibers smaller than average in size. However, when such atrophy did occur it was often found in all of the fibers composing one or more fascicles. The changes might be attributed to the damage or section of one or more small nerve branches at the time of implantation. The stable enzyme profiles of fibers adjacent to the device suggested that damage did not occur selectively in any one fiber type and that the stimulation was relatively innocuous.

Further no differences were found between active and passive devices under the conditions of the study. It remains possible that active devices could produce more damage or changes in enzyme levels if they were used to stimulate the muscle for longer periods of time. Damage to muscles by prolonged stimulation can follow the improper or overenthusiastic use of any stimulator and can be produced even by vigorous natural exercise [23]. The regime adopted for the work described here is typical of protocols used elsewhere for clinical rehabilitation of spinal cord injured patients [24], [25].

In a single instance, we observed muscle-fiber damage that was unusual and might have been caused by muscle stimulation. This damage occurred in a semitendinosus muscle, a muscle known to be composed of in-series fibers [26]. We might speculate that the in-series architecture of the semitendinosus contributed to the development of this modest region of damage. In some series-fibered muscles, it is possible to stimulate more muscle fibers at one muscle end than the other [27], [28], by submaximal motor unit activation. Such asymmetrical activity has been shown to cause non-uniform length changes along the length of the muscle, so that muscle fibers at the weaker end must work under lengthening (eccentric) conditions. A range of physiological studies have shown that muscle damage is relatively common after vigorous eccentric contractions [29], [30]. Thus, stimulation of muscles in a pattern that might cause eccentric conditions in some muscle parts may set up shear forces that have a damaging effect, even if the device itself is biocompatible.

Most of the implanted materials or components that were studied produced a similar inflammatory response regardless of the size, shape, or composition. Only the broken glass pieces caused damage to cross-sectional areas of muscle greater than 1mm^2 and this response was

the only one that did not appear to resolve. Silicone tubing was found to produce the least amount of damage and to result in a capsule whose thickness was less than one fifth that of the reaction zone measured around the glass shards. The modest reaction to silicone tubing is consistent with previous studies that generally attribute its biocompatible nature to its benign chemical constituents. However, silicone tubing was also the softest material implanted and might have the least tendency to abrade moving muscle fibers during the vigorous contractions that hindlimb muscles can be expected to generate under free-ranging behavioral conditions.

Does the muscular target matter?

The thickness of the capsule around implanted stimulators did not vary significantly amongst the different muscles. However, several other features of the foreign-body response differed depending upon the type of muscle that was implanted. Tibialis anterior consistently showed the least severe response whereas soleus and medial gastrocnemius tended to exhibit greater responses. The reasons for such differences cannot be determined from this type of study. Nevertheless, we might speculate that the severity of muscle reaction may be related to the architecture and activity level of the muscle into which the device is implanted. The usage patterns of cat hindlimb muscles are known to differ substantially even though their fiber-type compositions are often similar. For example Ariano [31] has shown that MG and TA both have approximately 60 % fast-glycolytic and 20 % slow-oxidative fibers. However, MG is an extensor and is active during standing and the stance phase of walking from heel strike to toe release, whereas TA is a flexor and active mostly while shortening is unopposed during the swing phase of walking from toe release to heel strike [32]. During normal walking the stance

phase has been found to last twice as long as the swing phase. The more continual contractions and higher forces in MG might lead to a greater mechanical abrasion of muscle tissue around the rigid implanted device. Alternatively, the varying degree of damage that is seen in different host muscles may relate to some intrinsic, but as yet poorly understood feature of muscle structure and performance. For example, Lexell et al. [33] has raised the possibility that stimulation-induced damage can vary in a manner related to muscle architecture. He electrically stimulated rabbit TA and EDL muscles at several different frequencies under essentially identical conditions and found that damage in EDL was consistently greater than in TA, for all frequencies.

The finding that muscles show differences in their foreign-body reactions is an important observation for protocols that aim to evaluate the biocompatibility of devices for regulatory or other purposes. Most if not all biocompatibility testing is performed in conformance to standards developed using the paravertebral muscles of rabbits or the gluteal muscles of rats (ASTM Standards, Vol 13.01). Paraspinal muscles of sedentary or restrained animals may rarely be active and thus may not move repeatedly against the hard surfaces of an implanted device. In such a situation we might expect the most benign of muscle reactions. However, more damage might be expected if the same implanted device were to be inserted into a different, highly active muscle. By implanting devices into the distal limb muscles of free-ranging cats, we feel the devices were subjected to a particularly severe biocompatibility challenge compared to responses reported by conventional testing. In the clinical environment, muscle stimulators such as those examined here will be implanted in muscles with a high degree of variation in their architectures,

usage patterns, age and health. All of these variable factors add a significant level of complexity when designing and testing a generic system that will be used for several applications.

ACKNOWLEDGMENTS

The authors acknowledge Dr. J. Rossitor for assistance in the analysis of the pathology, Janet Creasy for assistance in the preparation of the figures, Jennifer Conway for assistance in the statistical analysis, and the support of the Ontario Rehabilitation Technology Consortium, Canadian Neuroscience Network of Centres of Excellence, and U.S. National Institutes of Health research contract #N01-NS-2-2322 and N01-NS-5-2325

REFERENCES

- [1] G.E. Loeb, C.J. Zamin, J.H. Schulman, and P.R. Troyk, "Injectable microstimulator for functional electrical stimulation," *Med. & Biol. Eng. & Comput.*, vol 29, pp.13-19, 1991.
- [2] T. Cameron, G.E. Loeb, R.A. Peck, J.H. Schulman, P. Strojnik, and P.R. Troyk, "Micromodular implants to provide electrical stimulation of paralyzed muscles and limbs," *IEEE Trans. on Biomed. Eng.*, (in press).

T. Cameron, G.E. Loeb, F.J.R. Richmond, R.A. Peck, J.H. Schulman, P. Strojnik, and P. Troyk, "Micromodular electronic devices to activate paralyzed muscles and limbs" *Proceedings of the IEEE EMBS*, vol 15, pp. 1242-1243, Oct. 1993.
- [3] S.C. Woodward, and T.N. Salthouse, "The tissue response to implants and its evaluation by light microscopy," In *Handbook of Biomaterials Evaluation*, Edited by A.F. Von Recum, Macmillan Publishing Company, New York, pp. 364-377, 1986.
- [4] R.E. Baier, and R.C. Dutton, "Initial events in interactions of blood with a foreign surface," *J. Biomed. Mater. Res.*, vol 3, pp. 191-206, 1969.
- [5] V.I. Sevastianov, "Role of protein adsorption in blood biocompatibility of polymers," *CRC Crit. Rev. Biocompat.*, vol 4, pp. 109-154, 1988.
- [6] J.D. Andrade, and V.L. Hlady, "Plasma protein adsorption: The big twelve," *Ann. N.Y. Acad. Sci.*, vol 516, pp. 158-172, 1987.
- [7] D.F. Williams, "Standard tests for soft tissue evaluation," In *Biomaterials and Clinical Applications*, Edited by A. Pizzoferrato, P.G. Marchetti, A. Ravaglioli, and A.J.C. Lee, Elsevier Science Publishers B.V., Amsterdam, pp. 783-790, 1987.

- [8] K. Kottke-Marchant, J.M. Anderson, Y. Umemura, and R.E. Marchant, "Effect of albumin coating on the in vitro blood compatibility of Dacron arterial prostheses," *Biomaterials*, vol 10, pp. 147-155, 1989.
- [9] L. Tang, and J.W. Eaton, "Fibrin(ogen) mediates acute inflammatory responses to biomaterials," *J. Exp. Med.*, vol 178, pp. 2147-2156, 1993.
- [10] B. Weiss, R. Stickler, S. Schider, and H. Schmidt, "Corrosion fatigue testing of implant materials (Nb, Ta, stainless steel) at ultrasonic frequencies," *Proceedings of the first international conference on fatigue and corrosion fatigue up to ultrasonic frequencies*, Warrendale, PA, Metallurgical Society of AIME, pp. 387-411, 1982.
- [11] H. Zitter, and H. Plenck Jr, "The electrochemical behavior of metallic implant materials as an indicator of their biocompatibility," *J. Biomed. Mater. Res.*, vol 21, pp. 881-96, Jul. 1987.
- [12] S.M. Slack, and T.A. Horbett, "The effects of temperature and buffer on fibrinogen adsorption from plasma to glass," *J. Biomat. Sci., Polymer Ed.*, vol 2, pp. 227-37, 1991.
- [13] J.S. Walter, J. McLane, W. Cai, T. Khan, and S. Cogan, "Evaluation of a thin-film peripheral nerve-cuff electrode," *J. Spinal Cord Med.*, vol 18, pp. 28-32, 1994.
- [14] T.L. Fitzpatrick, T.L. Liinaamaa, I.E. Brown, T. Cameron, and F.J.R. Richmond, "A novel method to identify migration of small implantable devices, " *J. Long-term Effects of Med. Implants*, (in press)
- [15] Weatherford
- [16] L. Guth, and F.J. Samaha, "Qualitative differences between actomyosin ATPase of slow and fast mammalian muscle," *Exp. Neurol.*, vol 25, pp. 138-152, 1969.

- [17] T.N. Salthouse, and B.F. Matlaga, "Some cellular effects related to implant shape and surface," In *Biomaterials in reconstructive surgery*, Edited by L.R. Rubin, C.V. Mosby Company, St Louis, pp. 40-45, 1983.
- [18] D.L. Guyton, and F.T. Hambrecht, "Theory and design of capacitor electrodes for chronic stimulation," *Med. and Biol. Eng.*, vol 12, pp.613-620, 1974.
- [19] I. Carr, *The Macrophages*, Academic Press. New York, pp. 1-60, 1972.
- [20] S.L. Robins, and R.S. Cotran, *Pathologic Basis of Disease*, 2nd edition, Saunders, Philadelphia, pp. 94-95, 1979.
- [21] T.J. Chambers, "Multinucleate giant cells," *J. Pathol.*, vol 126, pp. 125-148, 1978.
- [22] D.L. Guyton, and F.T. Hambrecht, "Capacitor electrode stimulates nerve or muscle without oxidation-reduction reaction," *Science*, vol 181, pp. 74-76, 1973.
- [23] S. Salmons, "Exercise, stimulation and type transformation of skeletal muscle," *Int. J. Sports Med.*, vol 15, pp. 136-141, 1994.
- [24] A. Kralj, and T. Bajd, *Functional Electrical Stimulation, Standing and Walking After Spinal Cord Injury*, Boca Raton, FL, CRC, 1989.
- [25] R.B. Stein, T. Gordon, J. Jefferson, A. Sharfenberger, J.F. Yang, J. Totosy de Zepetnek, and M. Belanger, "Optimal stimulation of paralyzed muscle after human spinal cord injury," *J. Neurophysiol.*, vol 72, pp. 1393-1400, 1992.
- [26] E. Smits, P.K. Rose, T. Gordon, and F.J.R. Richmond, "Organization of single motor units in feline sartorius," *J. Neurophysiol.*, vol 72, pp. 1885-1896, 1994.
- [27] S.H. Scott, D.B. Thomson, F.J.R. Richmond and G.E. Loeb, "Neuromuscular organization of feline anterior sartorius: II. Intramuscular length changes and complex

length-tension relationships during stimulation of individual nerve branches," *J. Morphol.*, vol 213, pp. 171-183, 1992.

- [28] D.B. Thomson, S.H. Scott, and F.J.R. Richmond, "Neuromuscular organization of feline anterior sartorius: I. Asymmetric distribution of motor units," *J. Morphol.*, vol 21, pp. 147-162, 1991.
- [29] R.L. Lieber, and J. Friden, "Muscle damage is not a function of muscle force but active muscle strain," *Amer. Physiol. Soc.*, vol 74, pp. 520-526, 1993.
- [30] T.M. Best, C.T. Hasselman, and W.E. Garret, "Clinical aspects and basic science of muscle strain injuries," *BAM*, vol 4, pp. 77-90, 1994.
- [31] M.A. Ariano, R.B. Armstrong, and V.R. Edgerton, "Hindlimb muscle fiber populations of five mammals," *J. Histochem. Cytochem.*, vol 21, pp. 51-55, 1973.
- [32] L.D. Abraham, and G.E. Loeb, "The distal hindlimb musculature of the cat," *Exp. Brain Res.*, vol 58, pp. 580-593, 1985.
- [33] J. Lexell, J. Jarvis, D. Downham, and S. Salmons, "Stimulation-induced damage in rabbit fast-twitch skeletal muscles: a quantitative morphological study of the influence of pattern and frequency," *Cell Tissue Res.*, vol 273, pp. 357-362, 1993.

LIST OF FIGURES

- Figure 1. Line drawing of the terminal experimental preparation showing the location of the microstimulator with respect to muscle landmarks. The proximal end of the muscle is attached to a force transducer.
- Figure 2. Threshold settings (normalized to day one) as a function of time (days post-implantation). Thresholds were measured weekly for the duration of the experiment.
- Figure 3. Photomicrographs of an implantation site in the medial gastrocnemius muscle that contained an active device. Tissue sections were stained with hematoxylin and eosin. A. Typical features of the capsule and cellular response visualized at low magnification; B. a high magnification of the fibrous capsule and cellular response; C. a region of abnormally small muscle fibers at the edge of the capsule with centrally located nuclei.
- Figure 4. Cumulative frequency as a function of capsule thickness (mm) for active devices, passive devices, and suture material. The dotted line shows the median size of capsule. Insert shows the capsule thickness (score) as a function of muscle type for active and passive devices.
- Figure 5. Fibrosis score, cell score, and muscle-fiber score for active and passive devices as a function of muscle type; ξ - indicates a significant difference between muscles ($p < .05$). Fibrosis score was out of a maximum of four. Cell score was calculated by summing the five weighted individual cell scores giving a maximum score of 36. Muscle-fiber score was calculated by summing the weighted muscle score $< 100 \mu\text{m}$

with the weighted muscle score $> 100 \mu\text{m}$ giving a maximum score of 20. (See Table 4.2 for details) * - Note, the average muscle score for LG was zero.

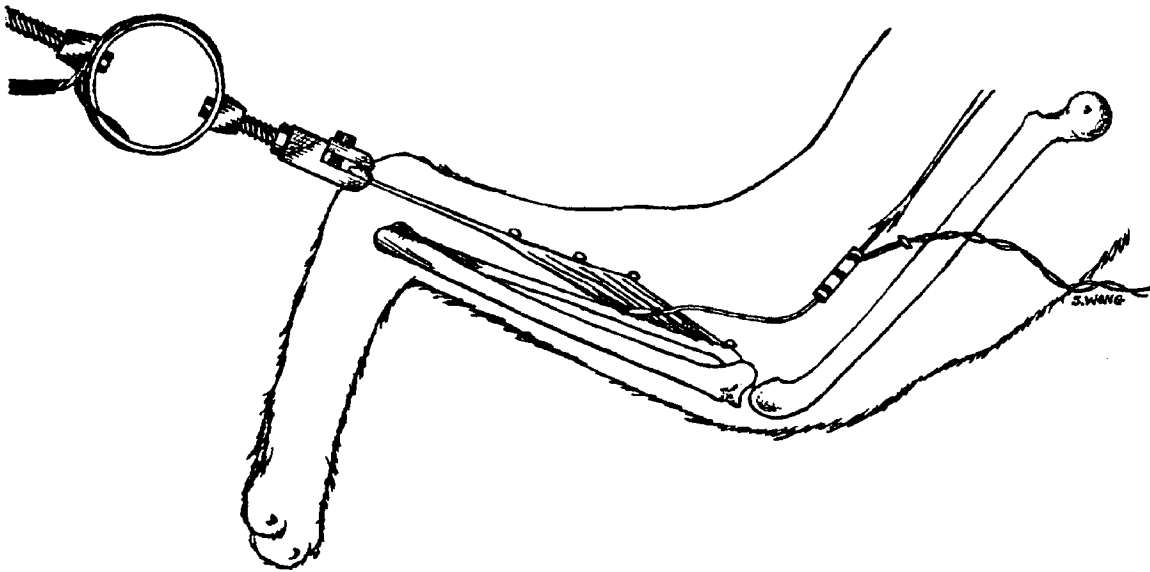
Figure 6. A. Cell score, fibrosis score, and muscle-fiber score for active and passive devices in the medial gastrocnemius muscle. Fibrosis score was out of a maximum of four. Cell score was calculated by summing the five weighted individual cell scores giving a maximum score of 36. Muscle-fiber score was calculated by summing the weighted muscle score $< 100 \mu\text{m}$ with the weighted muscle score $> 100 \mu\text{m}$ giving a maximum score of 20. (See Table 4.2 for details) B. Cell counts for active and passive device implants for the medial gastrocnemius muscle. (average of five sites) * - indicates a significant difference ($p < .05$) between active and passive implants.

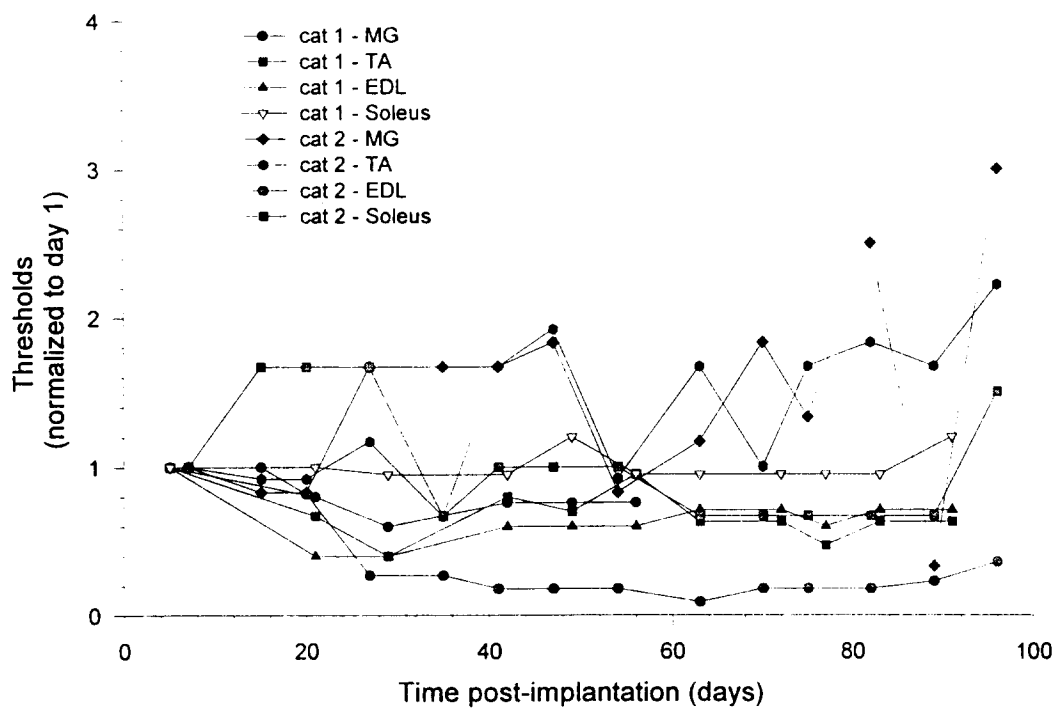
Figure 7. Capsule volume as a function of the implanted material. The capsule volume is largest for the broken glass pieces and smallest for the Silastic tubing. (n) - indicates the number of samples in each group.

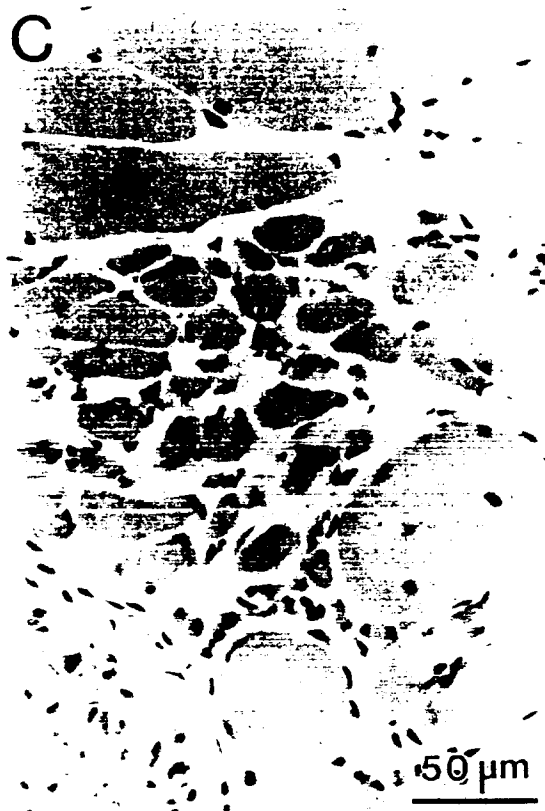
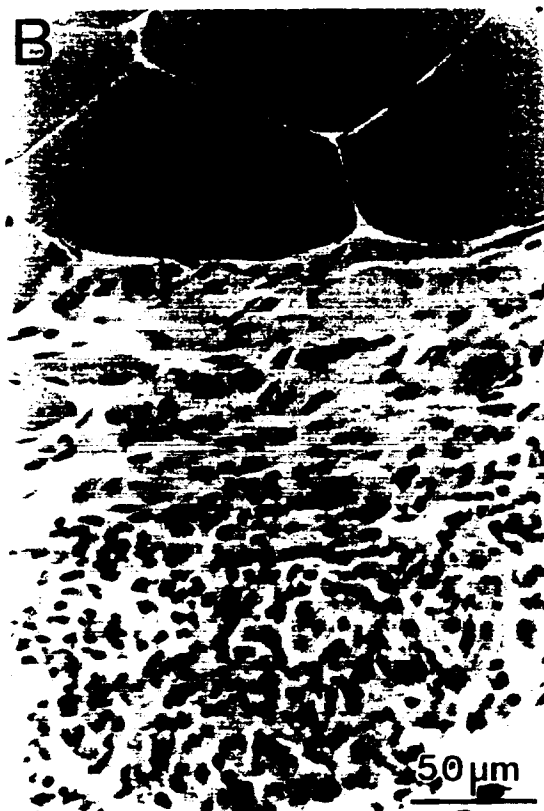
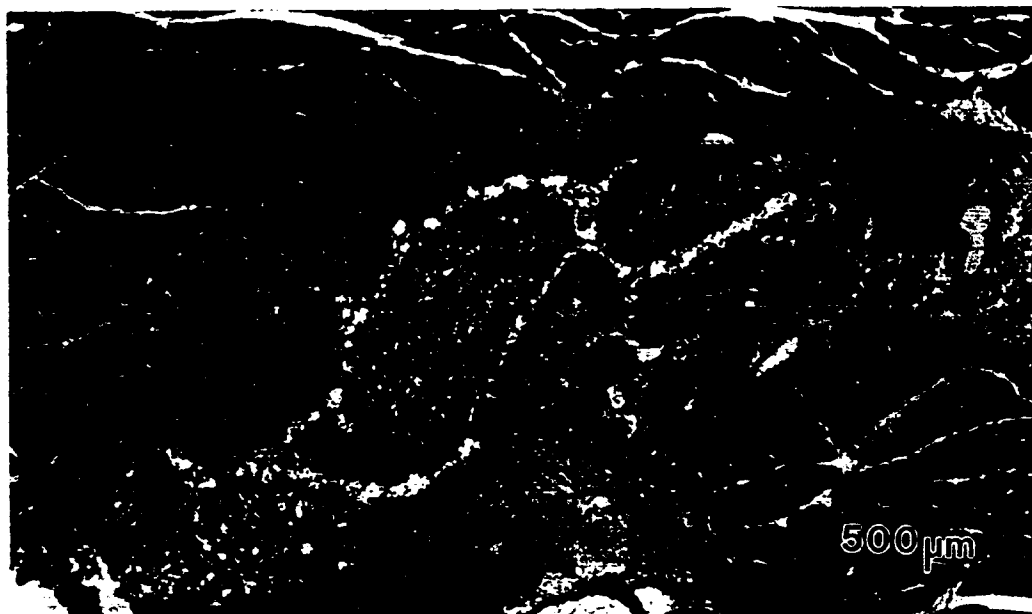
Figure 8. Diagram of the damaged region in the semitendinosus muscle with respect to the location of the stimulator. Insert A. Photomicrograph of the damaged site in the semitendinosus muscle proximal to the device; B. photomicrograph of the implantation site in the semitendinosus muscle stained with hematoxylin and eosin in the region around the active device.

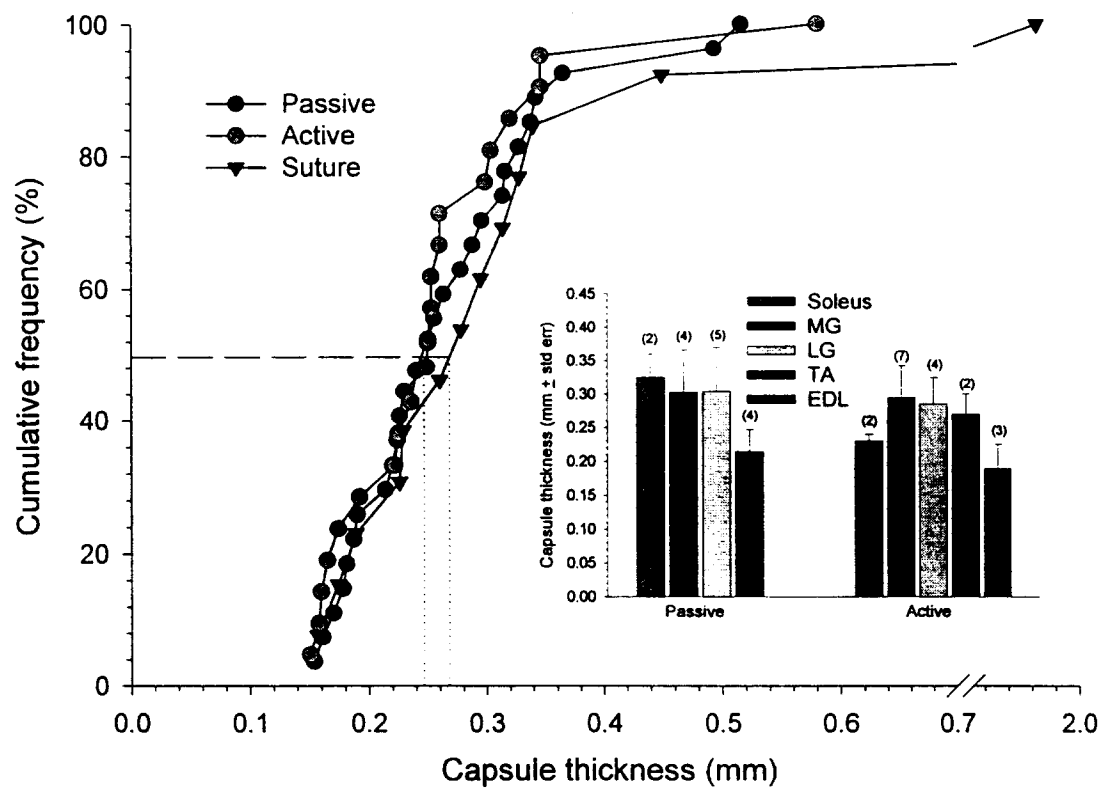
Table 9. A. List of the animal number, location of implant, duration of implant, duration of stimulation and initial threshold values for each cat implanted with active devices. B. List of the animal number, location of implant, and duration of implant for each cat implanted with passive devices, materials, and stimulator components.

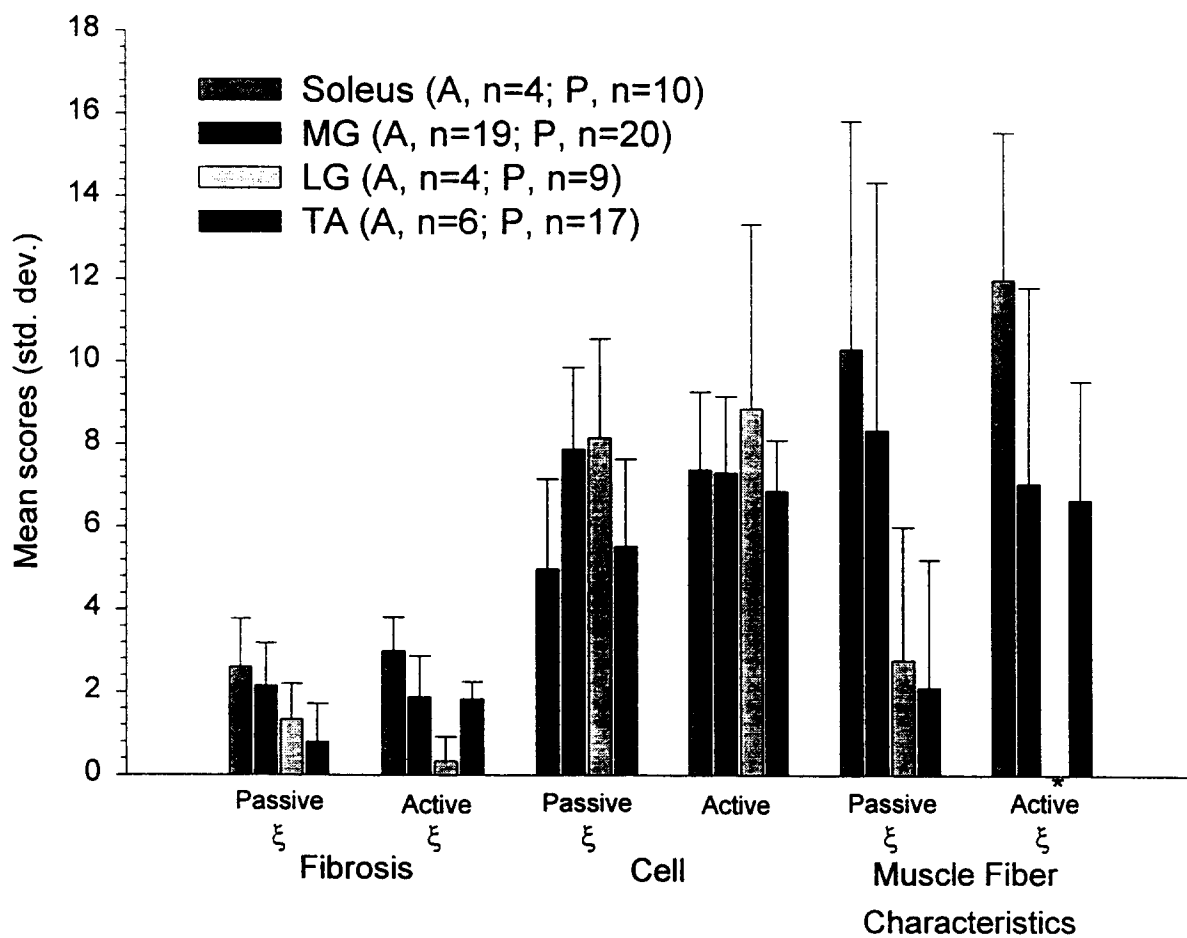
Table 10. Scoring key used the in analysis of tissue implanted with active and passive devices, components, and other materials.

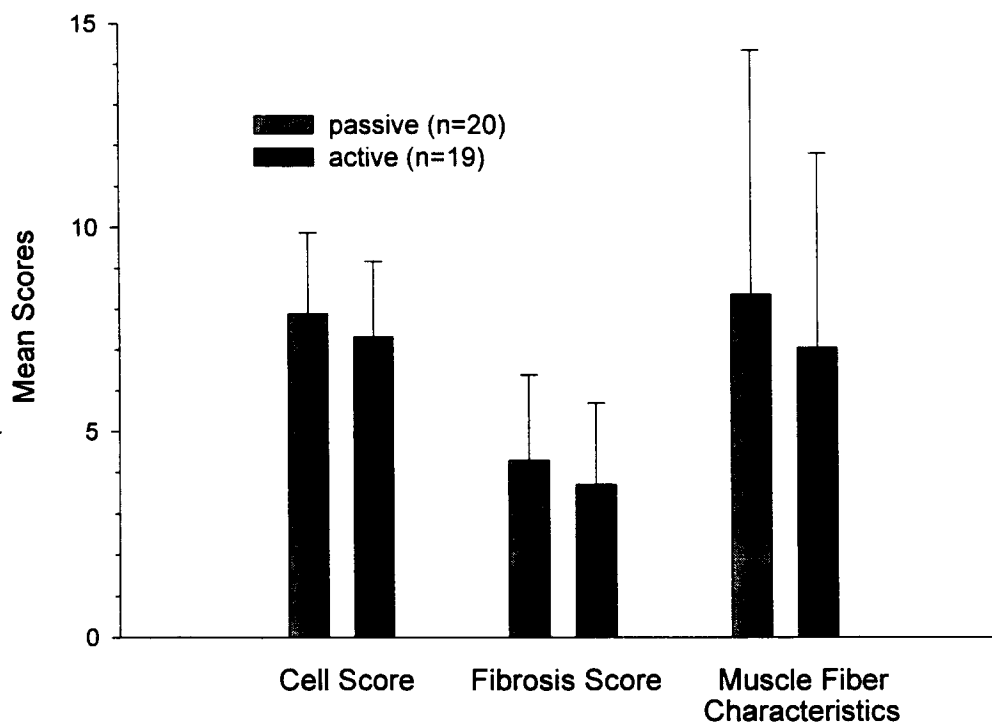
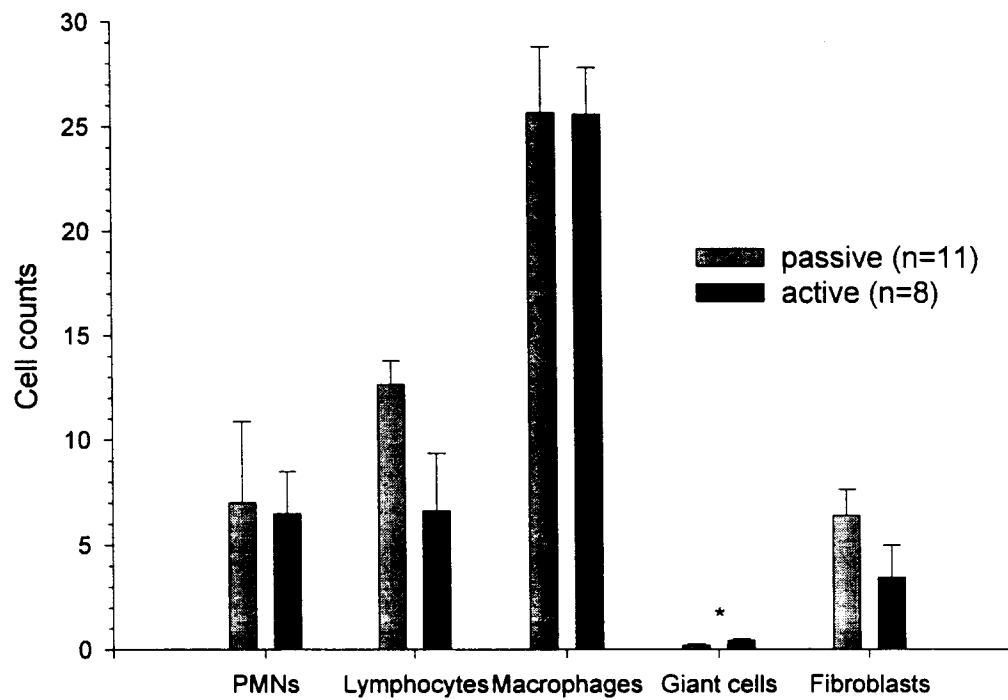


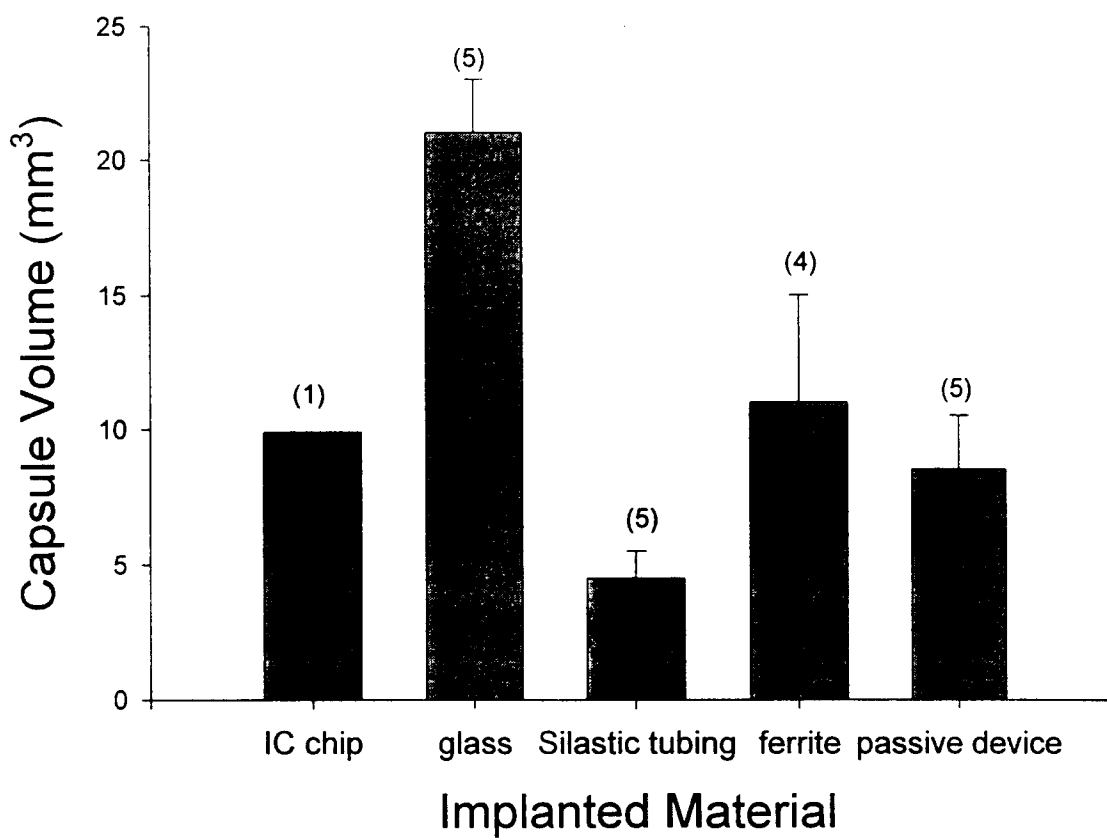












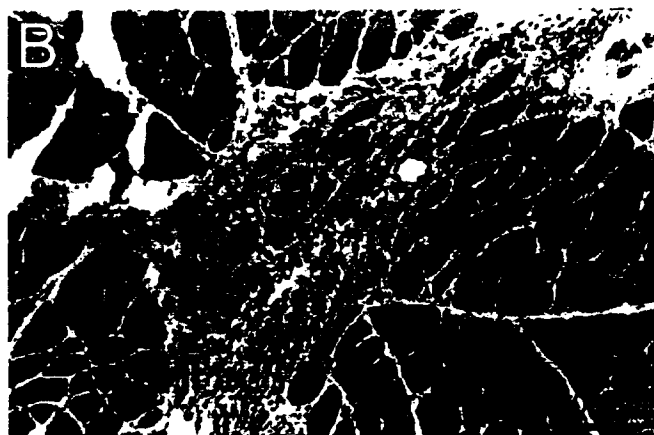
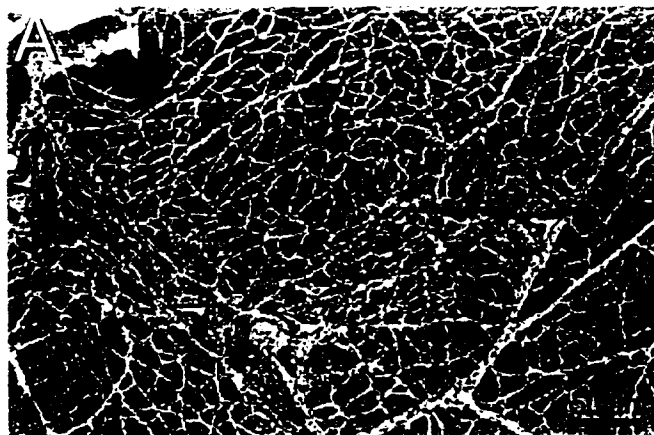
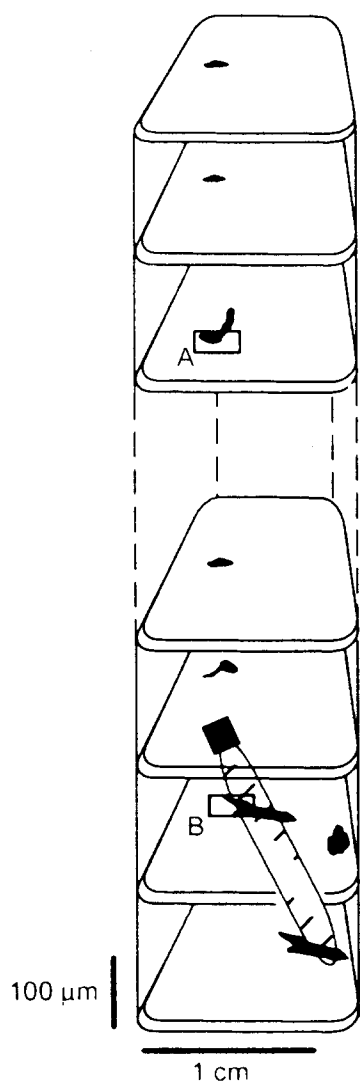


Table 9

Implant Location (cat : muscle)	Device ID #	Implant duration/ stimulation days	Initial Threshold	
			Current (mA)	Pulse Width (msec)
Max: R soleus	052 / 85	101 / 65	0.4	100
Max: R nerve medial gastrocnemius	053 / 1	101 / 37	1.0	100
Max: R tibialis anterior	037 / 4	101 / 65	0.6	100
Max: R extensor digitorum longus	054 / 5	101 / 65	0.8	100
Percy: R soleus	055 / 85	105 / 69	0.4	60
Percy: R nerve medial gastrocnemius	058 / 6	105 / 69	0.4	50
Percy: R tibialis anterior	059 / 63	105 / 69	1.2	120
Percy: R extensor digitorum longus	057 / 255	105 / 69	0.8	110
Biawy: R posterior biceps femoris	060 / 6	56 / 30	0.6	120
Biawy: R semitendinosus	062 / 31	56 / 30	0.4	130
Biawy: R anterior sartorius	061 / 32	56 / 30	1.2	60
Biawy: R medial sartorius	056 / 85	56 / 30	1.6	130

Implant Location (cat : muscle)	Material	Implant duration (days)
N144: R medial gastrocnemius	glass	30
N144: R lateral gastrocnemius	silicon tubing	30
N144: L medial gastrocnemius	ferrite	30
N144: L lateral gastrocnemius	intergrated circuit chip	30
N165: R medial gastrocnemius	intact stimulator	30
N165: R lateral gastrocnemius	silicon tubing	30
N165: L medial gastrocnemius	glass	30
N165: L lateral gastrocnemius	ferrite	30
N166: R medial gastrocnemius	intact stimulator	30
N166: R lateral gastrocnemius	silicon tubing	30
N166: L medial gastrocnemius	glass	30
N166: L lateral gastrocnemius	ferrite	30
N167: R medial gastrocnemius	intact stimulator	30
N167: R lateral gastrocnemius	silicon tubing	30
N167: L medial gastrocnemius	glass	30
N167: L lateral gastrocnemius	ferrite	30
N168: R medial gastrocnemius	intact stimulator	30
N168: R lateral gastrocnemius	silicon tubing	30

N168: L medial gastrocnemius	lass	30
N168: L lateral gastrocnemius	ferrite	30
Romeo: R (belly) lateral gastrocnemius	passive device	33
Romeo: L (belly) lateral gastrocnemius	passive device	33
Romeo: L (distal) biceps femoris	passive device	33
Romeo: R (distal) biceps femoris	passive device	33
Romeo: R Tibialis anterior	passive device	33
Romeo: R (belly) medial gastrocnemius	passive device	33
Romeo: R (nerve) medial gastrocnemius	passive device	33

Table 10

	Weight factor	1	2	3	4
PMNs	3	1-20	21-40	41-60	61+
Lymphocytes	2	1-20	21-40	41-60	61+
Macrophages	1	1-10	11-20	21-30	31+
Giant cells	2	1	2	3	4
Fibroblasts	1	1-10	11-20	21-30	31+
Capsule thickness	NA	0-.15 mm	.15-.3 mm	.3-.45 mm	.45+ mm
Muscle fiber characteristics (<100 μ m)	2	minimum	mild	moderate	severe
Muscle fiber characteristics (>100 μ m)	3	minimum	mild	moderate	severe
Fibrosis	NA	minimum	mild	moderate	severe

Cell counts were made within a 0.01 mm² area under 1000x magnification.